Journal of Engineering and Science Research 3 (4): 01-04, 2019
e-ISSN: 2289-7127

DOI: 10.26666/rmp.jesr.2019.1.4

# Improving photocatalytic decomposition by MWCNT and anodized α-Fe$_2$ O$_3$ composite

*Kosuke Kawakami , Dang Trang Nguyen, and Kozo Taguchi*
Department of Science and Engineering, Ritsumeikan University, Kusatsu, Shiga, Japan

**Abstract:** In recent years, photocatalytic technology has received attention for environmental protection. In this study, the usefulness of iron nanostructures generated by anodization was confirmed. Moreover, the synergistic effect of anodized iron (hematite, α-$Fe_2O_3$) and MWCNT (multi-walled carbon nanotube) was confirmed by methylene blue (MB) decomposition by MWCNT /α-$Fe_2O_3$ composite material. Electrophoretic deposition(EPD) was used as a method of making the MWCNT/α-$Fe_2O_3$ composite material. Characterization of the anodized samples and samples after EPD was performed by SEM and XRD, and concentration measurement of MB decomposition was performed using a spectrophotometer. The MB decomposition rate was improved in all the samples with MWCNT and the highest obtained with the MWCNT/α-$Fe_2O_3$ sample

**Key words:** *α-$Fe_2O_3$, Anodization, MWCNT, Photocatalytic degradation*

## INTRODUCTION

Today, photocatalytic technology has received attention for environmental protection. Iron oxide in its hematite crystalline structure is an interesting material for being used as photocatalyst for efficient degradation of organic pollutants as it has advantageous properties such as suitable band-gap (~2.1 eV), electrochemical stability, low toxicity and abundance [1]. However, the poor charge transportation in α- $Fe_2O_3$ has become a drawback. Nanostructuring techniques have been proven useful in increasing the performance of *a*-$Fe_2O_3$ for photo-response [2]. Takahashi has explored the photocatalytic decomposition of methylene blue by anodization iron oxides in different nanostructures, such as nanoparticle, nanorod, nanoporous and nanoleaflet, and has found that the nanoporous a-$Fe_2O_3$ layer showed the best photocatalytic performance [3]. As one of the most powerful techniques to fabricate self-organized and highly ordered nanostructure, anodization is widely investigated to form oxide nanotubes on so-called valve metals (Al, Ti, W, Nb, Zr) and their alloys over the last decade [4].

Moreover, a relatively newer method, to improve the charge transportation in nanostructured α-$Fe_2O_3$, is to modify its properties by introducing conducting materials such as carbon nanotube (CNT) [5]. Carbon nanotubes (CNTs) are attracting interest in research. And were considered as promising candidates for reinforcement in composite materials due to their excellent mechanical, electronic, magnetic, and gas adsorption properties. It was found that CNTs reinforced composites have prominent enhancement in the properties, such as hardness [6], bending strength, fracture toughness [7], wear resistance [8], corrosion resistance [9], electrical conductivity [10] and thermal stability [11]. Therefore, these properties make CNTs very useful for supporting $Fe_2O_3$ in many potential applications [12].

In this study, electrophoretic deposition (EPD) was used to make the MWCNT/α-$Fe_2O_3$ composite material. We confirmed the usefulness of iron nanostructures by anodic oxidation and the synergistic effect of anodized iron oxide (α-$Fe_2O_3$) and MWCNT was confirmed by methylene blue (MB) decomposition by MWCNT / α-$Fe_2O_3$ composite material.

**Corresponding Author:** Kozo Taguchi, Department of Electrical and Electronic Engineering, Ritsumeikan University, 1-1-1 Noji-Higashi, Kusatsu, Shiga 525-8577, Japan, email: taguchi@se.ritsumei.ac.jp

## EXPERIMENTAL

Iron foil (99.5%, 15 mm×20 mm, 1.0 mm thickness) was purchased from Nilaco Corporation(Japan). Ethylene glycol (EG), ammonium fluoride (NH4F), methylene blue, and ethanol were obtained from Wako Chemicals (Japan) without further purification. All solutions were prepared with deionized water.

The anodization was performed in a two-electrode electro-chemical cell with platinum being the cathode and the iron the anode under a constant DC voltage, using an electrolyte consisting of ammonium fluoride (96% purity) in an aqueous ethylene glycol (99.5% purity) solution. Fig. 1 shows a schematic diagram of two-electrode electro-chemical cell.

Prior to anodization, the surface of the iron foil was polished gradually with 240 to 2000 silicon carbide (SiC) papers and cleaned by sonication in ethanol for 10 min. After washing the sample with deionized water, electrochemical anodization was performed in an EG-based solution containing 0.5 wt% ammonium fluoride (NH4F) and 3 wt% water.

For the anodization, the volume of the electrolytic solution was 60 ml, and the applied voltage was 50 V for 6 minutes. The distance between Fe and Pt was 2.5 cm. After anodization, the as-anodized samples were properly washed with deionized water to remove the occluded ions and dried in oxygen atmosphere. Once the samples were dried, annealing was carried out at (T1) 400$^{O}$C in air for 2 h with heating and cooling rates of 2 °C/min and (T2) 600$^{O}$C in air for 6 h with heating and cooling rates of 1 °C/min.

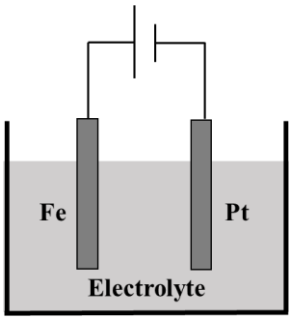


Fig. 1. schematic diagram of two-electrode electro-chemical cell

MWCNT (1wt%) was dispersed using an ultrasonic homogenizer for 20 minutes before EPD. For EPD, an aluminum substrate as a cathode and an anodized sample as an anode were fixed in parallel at 1 cm in the MWCNT suspension solution and a constant voltage of 30 V was applied for 90 seconds. the coated samples were carefully removed from the EPD solution and were dried in the air at room temperature for 2 hours. Subsequently, annealing was carried out at 400 $^{O}$C in the air for 1 h with heating and cooling rates of 2 °C/min.

The surface morphologies of a-$Fe_2O_3$ nanostructures were characterized by scanning electron microscopy (SEM) (HITACHI, SEM S-4300) with accelerated voltage of 5 keV. The crystalline structures and elemental composition of the as-anodized samples were characterized by X-ray diffraction (XRD) (PANalytical, X-ray Diffraction).

The photocatalytic activities of the as-anodized samples were evaluated by studying the degradation of MB in aqueous solution under illumination of fluorescent lamp (KL2681, MITSUBISHI). MB decomposition was measured at 680 nm for 2 hours with spectrophotometer every 30 minutes. Fig. 2 shows a schematic diagram of MB decomposition.

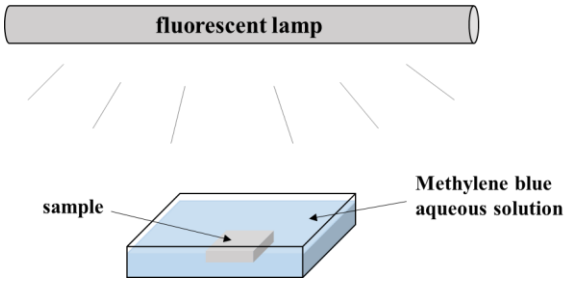


Fig. 2. schematic diagram of MB decomposition

## RESULTS AND DISCUSION

Fig. 3 (a), (b) shows SEM images of samples before EPD. The surface morphology of the sample of Fig. 3 (a) is the nanostructure of the $Fe_2O_3$ nanotube array obtained by T1 annealing condition. In this study, we could not obtain α-$Fe_2O_3$ nanotube array because the nanotube array collapsed when annealing at 500°C or higher to obtain α- $Fe_2O_3$. Fig. 3 (b) is an image of a sample having a high proportion of α-$Fe_2O_3$ achieved by T2 annealing condition. It is considered that crystallization was promoted by increasing the amount of water in the anodization solution and extending the annealing time. In this sample, reddish brown color peculiar to hematite (α-$Fe_2O_3$) appeared clearly.

Fig. 3 (c), (d) shows SEM images of samples after coating MWCNT by EPD. Fig. 3 (c) is an image of MWCNT / $Fe_2O_3$ nanotube array. It was observed that

MWCNT was covered much by the high surface area of the nanotube array. In this study, MWCNT (1 wt%) was used to make the same condition, but it is found that it is necessary to use low concentration when EPD is performed on nanotube array. Fig. 3 (d) is an image of MWCNT / α-$Fe_2O_3$. It turned out that MWCNT was modified to nanorods and nanoparticles

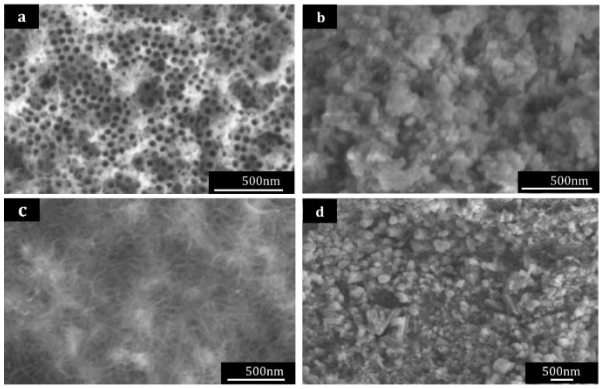


Fig. 3. SEM image of anodized samples before and after EPD. (a) $Fe_2O_3$ nanotube array, (b) α-$Fe_2O_3$, (c) MWCNT / $Fe_2O_3$ nanotube array, and (d) MWCNT / α-$Fe_2O_3$.

Fig. 4 shows the XRD pattern of $Fe_2O_3$ nanotube array and α-$Fe_2O_3$ after annealing and EPD. The α-$Fe_2O_3$ sample exhibited structural characteristic with pure rhombohedral symmetry of $Fe_2O_3$ (space group: R3c(167), a = 0.5035, b = 0.5035, c = 1.3748; JCPDS card No. 33-0664) indicating the crystalline hematite phase and absence of other impurity phase. The peaks at 24.12°, 33.17°, 35.60°, 40.91°, 49.41°, 53.98° and 62.56° are attributable to the hematite facet planes (012), (104), (110), (113), (024), (116) and (214), respectively. The peaks of (104) and (110) also contain α-$Fe_2O_3$ and $Fe_3O_4$.

There was no reaction of α-$Fe_2O_3$ in the $Fe_2O_3$ nanotube array sample. In order to eliminate the iron reaction, the temperature and time of annealing increased, but the nanotube array collapsed. The additional carbon peak at 2θ = 31.6 ° in the XRD pattern of the sample after EPD is due to the presence of MWCNT. Although there was a reaction of carbon in the XRD pattern of the two samples after EPD, there was no clear peak.

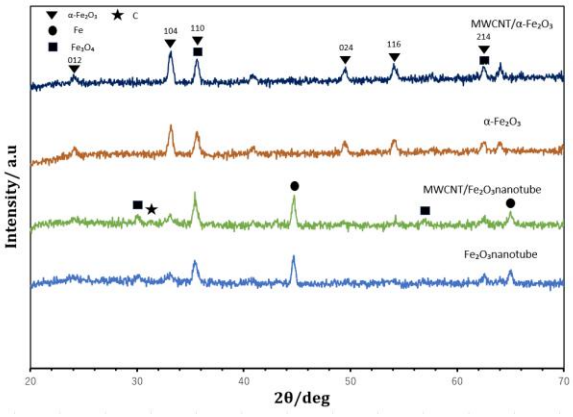


Fig. 4. XRD pattern of $Fe_2O_3$ nanotube array and α-$Fe_2O_3$ after annealing and EPD.

In general, MB is considered as a representative organic dye, and it can easily be monitored by optical absorption spectroscopy. MB is chosen as model contaminants to evaluate the photocatalytic activities of the samples due to its stability under visible light and near UV light. Fig.5 (a) and (b) are graphs of MB decomposition performed on samples before EPD and after EPD to coat MWCNT, respectively. The original iron foil without anodization (unprocessed iron) was also tested in this experiment.

From Fig. 5 (a), it was found that there is no optical response to the unprocessed iron. In contrast, $Fe_2O_3$ and α-$Fe_2O_3$ clearly show photocatalytic activity. Based on this result, it was confirmed that α-$Fe_2O_3$ is superior to $Fe_2O_3$ as a photocatalyst. In the graph of Fig. 5 (b), the decomposition speed was improved in all the samples with MWCNT coated by EPD. Among them, the decomposition rate of the decomposition speed of α-$Fe_2O_3$ was much improved. From this result, it was confirmed that the synergistic effect of the MWCNT / α-$Fe_2O_3$ composite on photocatalytic decomposition of MB.

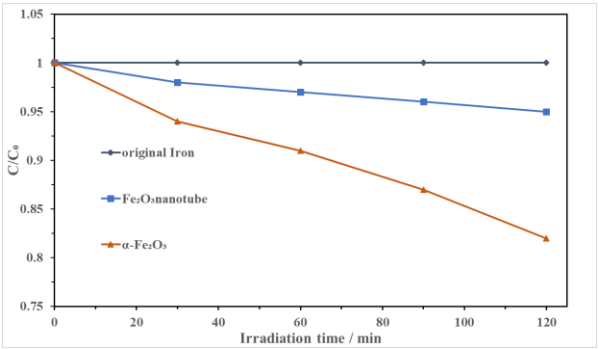


(a)

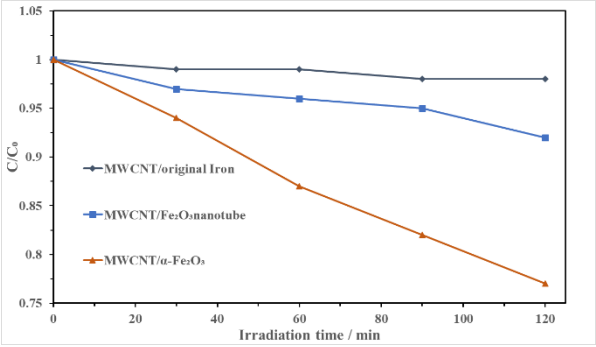


(b)

Fig. 5. Photocatalytic degradation of methylene blue on anodized samples and original iron. (a) before EPD and (b) after EPD.

## CONCLUTIONS

In this study, it was confirmed that the photocatalyst performance was improved by the synergistic effect of MWCNT and α-$Fe_2O_3$ obtained by anodization and EPD. It was also confirmed that the nanotube array has a large surface area based on the modification status of MWCNT of the SEM image after EPD. We will aim to improve the surface area and electron mobility by fabricating α-$Fe_2O_3$ nanotube arrays using 99.99% iron foil in the future.

## REFERENCES

[1] V. A. N. De Carvalho, R. A. D. S. Luz, B. H. Lima, F. N. Crespilho, E. R. Leite, and F. L. Souza, "Highly oriented hematite nanorods arrays for photoelectrochemical water splitting," *J. Power Sources*, vol. 205, pp. 525–529, 2012.

[2] Z. Zhang, M. F. Hossain, and T. Takahashi, "Self-assembled hematite (α-$Fe_2O_3$) nanotube arrays for photoelectrocatalytic degradation of azo dye under simulated solar light irradiation," *Appl. Catal. B Environ.*, vol. 95, no. 3–4, pp. 423–429, 2010.

[3] Z. Zhang, M. F. Hossain, and T. Takahashi, "Fabrication of shape-controlled α-$Fe_2O_3$ nanostructures by sonoelectrochemical anodization for visible light photocatalytic application," *Mater. Lett.*, vol. 64, no. 3, pp. 435–438, 2010.

[4] K. Xie, M. Guo, H. Huang, and Y. Liu, "Fabrication of iron oxide nanotube arrays by electrochemical anodization," *Corros. Sci.*, vol. 88, pp. 66–75, 2014.

[5] S. Rai, A. Ikram, S. Sahai, S. Dass, R. Shrivastav, and V. R. Satsangi, "Photoactivity of MWCNTs modified α-$Fe_2O_3$ photoelectrode towards efficient solar water splitting," *Renew. Energy*, vol. 83, pp. 447–454, 2015.

[6] X. Chen, G. Zhang, C. Chen, L. Zhou, S. Li, and X. Li, "Carbon nanotube composite deposits with high hardness and high wear resistance," *Adv. Eng. Mater.*, vol. 5, no. 7, pp. 514–518, 2003.

[7] G. D. Zhan, J. D. Kuntz, J. Wan, and A. K. Mukherjee, "Single-wall carbon nanotubes as attractive toughening agents in alumina-based nanocomposites," *Nat. Mater.*, vol. 2, no. 1, pp. 38–42, 2003.

[8] C. S. Chen, X. H. Chen, Zhiyang, W. H. Li, L. S. Xu, and B. Yi, "Effect of multi-walled carbon nanotubes as reinforced fibres on tribological behaviour of Ni-P electroless coatings," *Diam. Relat. Mater.*, vol. 15, no. 1, pp. 151–156, 2006.

[9] X. H. Chen, C. S. Chen, H. N. Xiao, F. Q. Cheng, G. Zhang, and G. J. Yi, "Corrosion behavior of carbon nanotubes-Ni composite coating," *Surf. Coatings Technol.*, vol. 191, no. 2–3, pp. 351–356, 2005.

[10] C. L. Xu, B. Q. Wei, R. Z. Ma, J. Liang, X. K. Ma, and D. H. Wu, "Fabrication of aluminum / carbon nanotube composites and their electrical properties," *Carbon N. Y.*, vol. 37, no. 5, pp. 855–858, 1999.

[11] S. H. Liao, C. H. Hung, C. C. M. Ma, C. Y. Yen, Y. F. Lin, and C. C. Weng, "Preparation and properties of carbon nanotube-reinforced vinyl ester/nanocomposite bipolar plates for polymer electrolyte membrane fuel cells," *J. Power Sources*, vol. 176, no. 1, pp. 175–182, 2008.

[12] C. sheng CHEN *et al.*, "Preparation and magnetic property of multi-walled carbon nanotube/α-$Fe_2O_3$composites," *Trans. Nonferrous Met. Soc. China (English Ed.)*, vol. 19, no. 6, pp. 1567–1571, 2009.